

Extreme Ultraviolet-Printability and Mechanistic Studies of Engineered Hydrogen Silsesquioxane Photoresist Systems

Ashish Rathore,* Ivan Pollentier, Maicol Cipriani, Harpreet Singh, Danilo De Simone, Oddur Ingólfsson, and Stefan De Gendt



Cite This: *ACS Appl. Polym. Mater.* 2021, 3, 1964–1972



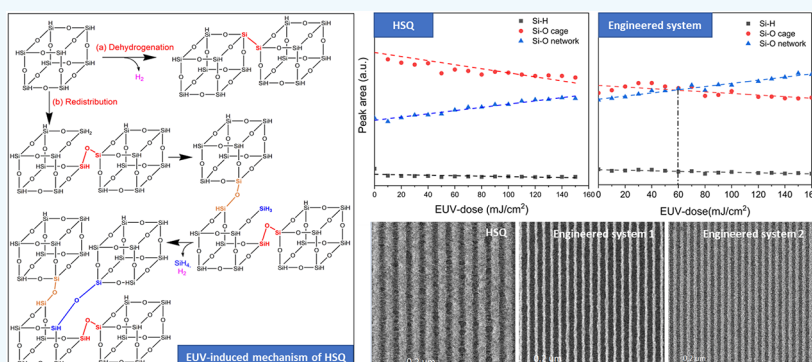
Read Online

ACCESS |

Metrics & More

Article Recommendations

Supporting Information



ABSTRACT: Hydrogen silsesquioxane (HSQ) photoresist has shown extremely high-resolution performance for electron-beam lithography and interference lithography and can be a potential photoresist candidate for extreme ultraviolet lithography (EUVL). To optimize this system for sub-10 nm patterning, it is important to understand the EUV- and electron-induced chemistry underpinning the functionality of this resist material. Here, we present an EUV-printability study on HSQ photoresist at resolutions of 16 and 22 nm combined with a mechanistic study on EUV- and electron-induced desorption of HSQ films. First, patterning results showed that the simple HSQ cages require a high EUV dose and an aggressive developer to print dense features. EUV- and electron-induced desorption experiments revealed that hydrogen and silane are the dominant species fragmented from HSQ, indicating dehydrogenation and redistribution pathways as the cross-linking mechanism. Quantum chemical calculations suggested that neutral dissociation is the dominant mechanism in HSQ cross-linking at low energies, i.e., below its ionization threshold, whereas dissociative ionization contributes significantly at higher energies. A distinct structure is observed at about 8 eV and a clear peak at about 11 eV, indicating a significant contribution through dissociative electron attachment at these energies. Based on these results, an engineered HSQ system is designed by adding silanol or carbinol ($R-CH_3OH$) groups to the partially cross-linked HSQ cages to increase its tetramethylammonium hydroxide (TMAH) developer and EUV sensitivity. Finally, 2.38% v/v TMAH is used to develop a 16 nm printed dense line-space with a line-edge roughness of 6.4 nm but requiring an EUV dose of over 100 mJ/cm².

KEYWORDS: EUV lithography, photoresist, light–matter interactions, EUV-induced mechanism, electron-induced mechanism, hydrogen silsesquioxane, alternative EUV-resist systems

1. INTRODUCTION

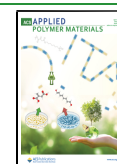
In the past few decades, chemically amplified resists (CARs) have been the primary photoresist system used in the lithography process. These resist systems worked well for the conventional deep-ultraviolet lithography (DUVL) process, which uses light with a wavelength of 193 nm (energy of ~6 eV) to print at a resolution down to 40 nm with a single patterning step. For further miniaturization, the semiconductor industry is quickly shifting from DUVL to extreme ultraviolet lithography (EUVL). The new process uses light with a wavelength of 13.5 nm (energy of ~91.6 eV) to print at sub-10 nm resolutions. However, transferring this new process to high-volume manufacturing (HVM) is proven to be problem-

atic, mainly because of the inefficient performance of the conventional CAR photoresist system. Several reasons have been identified for this exacerbated performance. First, due to the energy differences of the source radiation, light–matter interactions in the photoresist film change from excitation chemistry in the DUVL process to radiation chemistry in the

Received: January 12, 2021

Accepted: February 18, 2021

Published: March 4, 2021



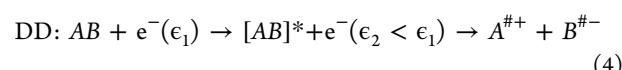
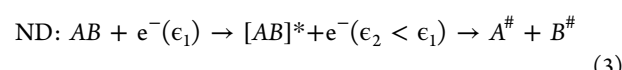
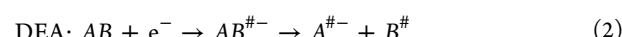
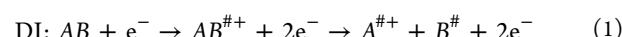
EUVL process.^{1–4} Also, despite a substantial effort to understand this in previous studies,^{5–9} the details of the EUV light–photoresist interactions are currently unclear. Second, the CAR platform patterns through an acid diffusion process, which is difficult to control. This causes problems such as high line-edge roughness (LER) and stochastic failures in the patterns.¹⁰ Third, the CAR system consists of multiple components such as a base polymer, photoacid generator, quencher, etc., which complicates the patterning process.¹¹ Because of all the aforementioned problems with the conventional CAR system, it is necessary to develop and optimize new photoresist systems with a simpler patterning mechanism for the EUVL process.

There have been many alternative resist systems reported for EUV lithography in recent years. Metal-based (Sn, Zn, Hf, Zr, Ti, and others) inorganic systems have gained a lot of attention, especially due to their enhanced EUV sensitivity and smaller molecular sizes.^{12–20} However, most of them are still in the research and development phase and their patterning data on a commercial EUV scanner is not available. The one standout EUV resist among all has been the Sn-based system developed by Inpria Corporation, which showed a resolution of 13 nm at a dose of 35 mJ/cm².²¹

Another promising system is the negative tone inorganic-based molecular resist system called hydrogen silsesquioxane (HSQ). HSQ is a popular high-resolution electron-beam lithography (EBL) resist already being used to print sub-10 nm dense features.^{22,23} Along with its high-resolution capabilities, the SiO₂-type composition of the HSQ patterns has a much higher modulus and shows less pattern collapse compared to the organic-based resist systems. The SiO₂-type composition also provides pattern selectivity to an array of materials.^{23–25} Because of all these advantageous litho-properties, HSQ is an interesting material for the EUVL process.

Previous EUV-patterning studies on HSQ resist with interference lithography (IL) have shown that sufficient cross-linking can be induced with an extremely high EUV dose of 4000–8000 mJ/cm² to resolve line-space (L/S) patterns of up to 6 nm HP.²⁶ A more recent study²⁷ with the commercial EUV scanner ASML NXE3300B reported patterns of 10 nm 1:2 L/S with an EUV dose of 60–70 mJ/cm². However, resolving the dense 1:1 L/S patterns was shown to be difficult even with longer development times using the semiconductor industry-standard positive tone developer (PTD), 2.38% v/v aqueous tetramethylammonium hydroxide (TMAH) solution.

There have also been studies to understand the thermal- and electron-induced cross-linking mechanisms for HSQ.^{28–30} However, the accurate light–matter interactions during EUV exposure are currently unclear. Also, when the resist is exposed to a high energy EUV photon, secondary electrons are generated in the film, which induces litho-chemistries based on certain electron-induced fragmentation mechanisms,³¹ namely, (1) dissociative ionization (DI), (2) dissociative electron attachment (DEA), (3) neutral dissociation (ND), and (4) dipolar dissociation (DD), as shown in eqs 1–4. Here, “#” represents that the transient species could be in a vibrationally and/or electronically excited state, whereas “*” represents an electronically excited state. ϵ_1 and ϵ_2 represent the energy of the secondary electrons generated in the film before (ϵ_1) and after (ϵ_2) energy transfer to the respective molecule.



Understanding the extent and nature of this electron-induced chemistry involved in the HSQ resist performance may allow for better optimization and enhanced EUV printability.

In this work, a high-resolution EUV-printability and mechanistic study of a simple HSQ resist is carried out. Based on the results obtained on the simple system, the chemistry of HSQ cages is modified to engineer better EUV systems. Chemical characterization and litho-results of the improved systems are also discussed.

2. RESULTS AND DISCUSSION

2.1. EUV-Printability and Mechanistic Studies of Simple HSQ Systems. **2.1.1. Contrast Curve and EUV-Printability Analysis.** A contrast curve of HSQ was checked for different development times using the industry-standard positive tone developer (PTD), 2.38% v/v TMAH, to find the best patterning conditions (Figure 1). The shape of the

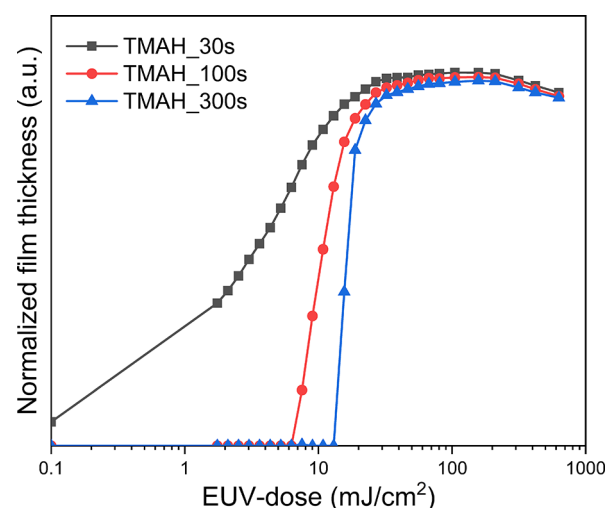


Figure 1. Contrast curve of HSQ resist for 2.38% v/v TMAH with development times of 30, 100, and 300 s.

contrast curve confirmed that the coated material is initially soluble in the TMAH developer but becomes insoluble after EUV exposure. Moreover, 300 s of development showed the best image contrast compared to 30 and 100 s development times with a dose-to-gel of 14.1 mJ/cm², which is close to the previously reported value of 11.5 mJ/cm² obtained on a 70 nm-thick film developed with 2.3% v/v TMAH for 120 s.³² This suggests that the image contrast improves with increasing development time within the time range studied. Furthermore, at a dose range of 100 mJ/cm² and above, there was a constant reduction in the film thickness due to film densification as a combined result of cross-linking, complete removal of moisture, and removal of volatile species.

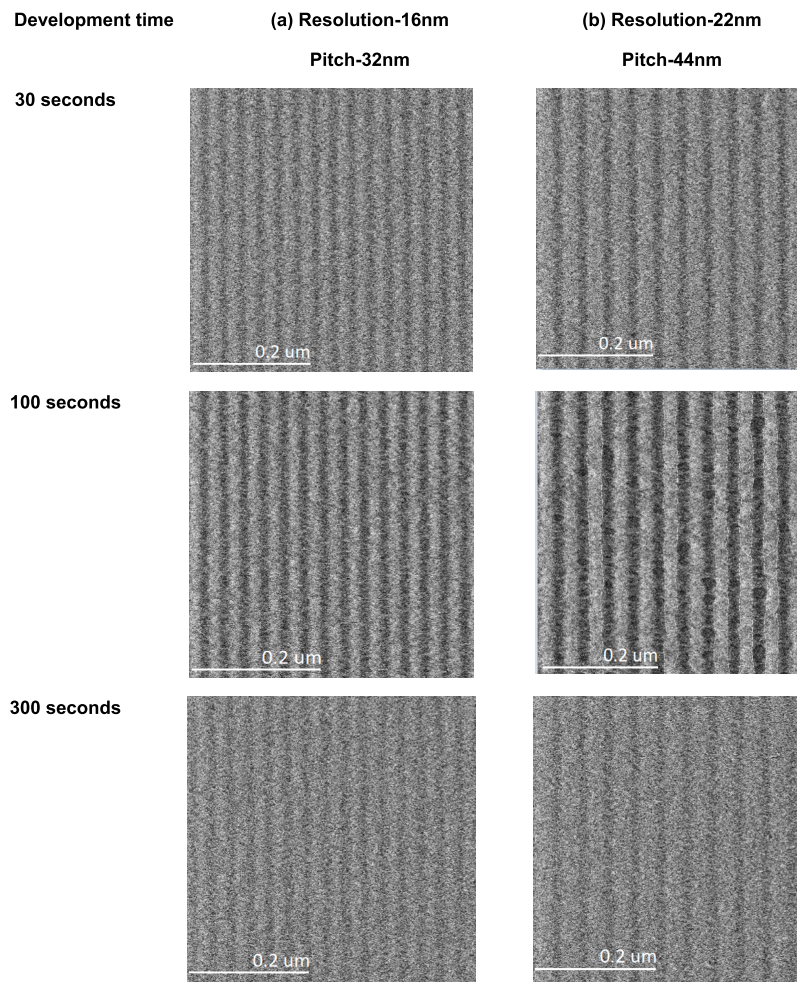


Figure 2. SEM images (at 100K magnification) to check the EUV printability of the 20 nm HSQ film for (a) 16 nm and (b) 22 nm dense L/S patterns with std. 2.38% TMAH development times of 30, 100, and 300 s.

Next, EUV printability on the 20 nm-thick HSQ resist film was checked at 16 and 22 nm L/S by exposing it to a dose of 70 mJ/cm² in an Imec's ASML NXE3300B scanner, and the SEM images are presented in Figure 2. The SEM images showed that the 100 s development time yields the best image contrast compared to 30 and 300 s. Upon further inspection, it was also noticed that the L/S patterns are more clearly defined for 100 s development time compared to both 30 and 300 s. This is contradictory to what was observed in the contrast curve previously, but the reason behind losing image contrast at very long development times (300 s) is that some portion of the cross-linked (patterned) part is also removed along with the unexposed part. Therefore, when using 2.38% v/v TMAH for HSQ resist, 100 s seems to be the optimum development time.

Upon further inspection of the SEM images in Figure 2, it was clear that the dense L/S patterns were not completely resolved, i.e., the spaces were not rendered clean after the development process. This is further shown in Figure S2 in the Supporting Information, where the dense (1:1 L/S) patterns are not resolved (Figure S2a) but the relaxed patterns (1:1.6 L/S) are starting to open up (Figure S2b), which suggests that the standard 2.38% v/v TMAH is not potent enough for high-resolution patterning of HSQ resist. It is known that the unexposed HSQ cages solubilize by forming silanol (Si—OH) groups when submerged in the TMAH developer solvent.³³

However, 2.38% v/v TMAH does not have the potency to convert enough Si—H bond to Si—OH bonds and solubilize the HSQ molecule. Another reason for unresolved spaces could be the scattering of secondary electrons from the exposed to unexposed regions of the photoresist film and inducing partial cross-linking in the HSQ molecules. Therefore, it is important to either improve the developer sensitivity of HSQ cages or apply a stronger developer solvent to resolve high-resolution patterns.

2.1.2. EUV-Induced Desorption and FTIR Spectroscopy of HSQ Films. To further understand the inability of HSQ resist to print at high resolutions with EUV lithography, it is important to understand the fundamental EUV- and electron-induced chemistry driving the patterning process. EUV/electron-induced desorption and FTIR studies can provide concrete ideas on the cross-linking mechanism of the HSQ molecules and may suggest ways to further improve its patterning performance.

From the contrast curve (Figure 1), an EUV dose of 30 mJ/cm² was chosen (a dose higher than the observed dose-to-gel) to expose a freshly coated 40 nm-thick HSQ film. The mass fragmentation plot indicating the neutral desorption species is presented in Figure 3. The two major desorption species obtained were *m/z*-32 and *m/z*-2, which can be assigned as silane (SiH₄) and hydrogen (H₂), respectively. Some traces of disilane ions (*m/z*-62) were also detected. Based on the

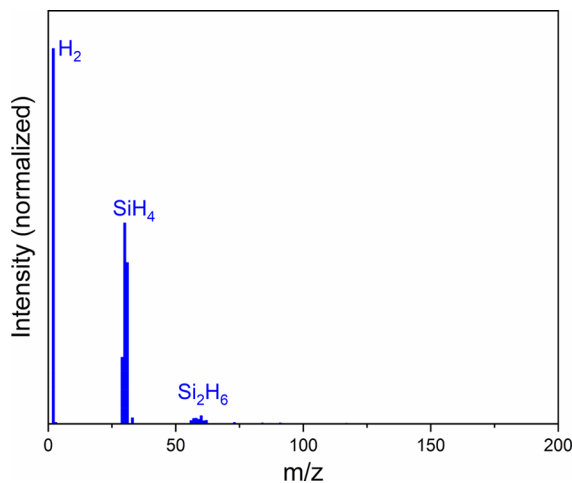


Figure 3. EUV-induced mass fragmentation of the 40 nm HSQ film exposed to a dose of 30 mJ/cm^2 .

observed desorption, EUV-induced cross-linking pathways are proposed for the HSQ resist, as shown in Figure 4.

There are two major types of cross-linking pathways that may occur when the HSQ cages are exposed to EUV radiation, as has been observed previously in temperature- and electron-induced mechanistic studies.^{28,29} The first major pathway is through the dehydrogenation process (Figure 4a), in which the intermolecular Si–H bond breaks and the adjacent cages can cross-link directly through intramolecular Si–Si bonding, with the evolution of H_2 gas. The second major pathway is called the cage redistribution pathway, which is indicated in Figure 4b. During this, the EUV photons break the intermolecular Si–O bonds to open up the cages, which facilitate intramolecular Si–O–Si linkages. The cross-linking reaction might happen in a stepwise manner with intermolecular hydrogen transfer (H_2 desorption) to form terminal Si–H, Si– H_2 , and Si– H_3 , eventually triggering the desorption of SiH_4 . Although both dehydrogenation and redistribution reactions induce cross-linking in HSQ cages, the redistribution reaction seems to be the dominant pathway as it produces both H_2 and SiH_4 , as is observed in the desorption experiments.

The occurrence of the redistribution pathway was further studied by FTIR spectroscopy. Based on its structural configuration,^{29,34} the Si–H stretching peak appears at 2200

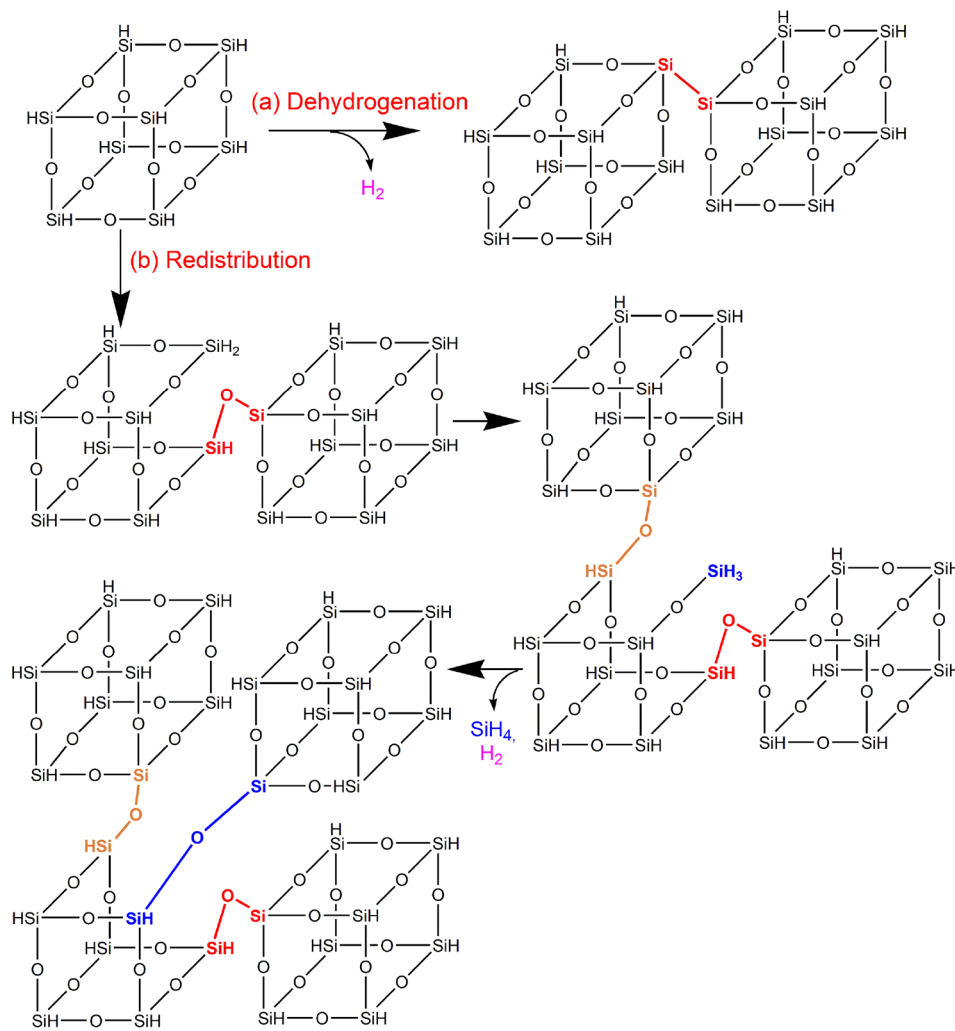


Figure 4. Two major pathways are anticipated in EUV-induced cross-linking of HSQ cages: (a) dehydrogenation reaction, where the two HSQ cages cross-link via direct Si–Si bonding, with the evolution of hydrogen gas, and (b) redistribution reaction, during which the cages open up and cross-link via Si–O–Si linkages, with the evolution of hydrogen and silane gas.

cm^{-1} , the Si—O—Si stretching mode signifying the cage configuration appears at approximately 1150 cm^{-1} (referred to as the Si—O cage peak hereafter), and the Si—O₂ vibrational mode signifying the network configuration appears at approximately 1070 cm^{-1} (referred to as the Si—O network peak hereafter). The aforementioned peaks are shown in the FTIR spectrum displayed in Figure S3 in the Supporting Information.

Figure 5 shows the evolution of the calculated FTIR peak areas observed when an HSQ film is exposed to an EUV dose

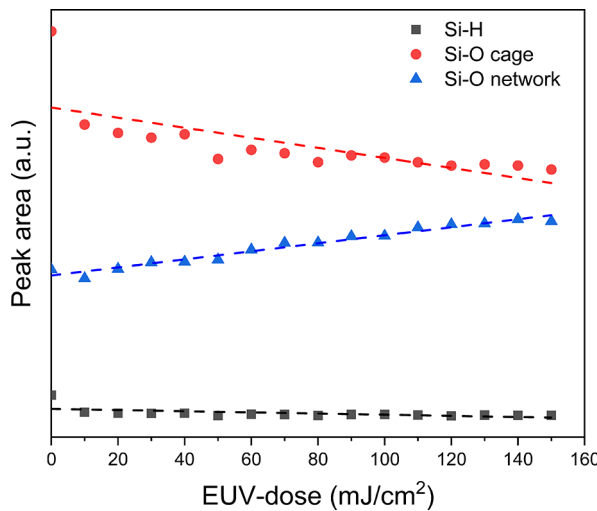


Figure 5. Variations in Si—H, Si—O (cage), and Si—O (network) peak areas w.r.t. the EUV dose.

of $0\text{--}150 \text{ mJ/cm}^2$. The Si—H peak area showed a slight decrease with increasing dose, signifying the loss of H-groups from the cages. The Si—O cage peak area showed a significant reduction, and the Si—O network peak area showed a proportional increase in its peak area. This confirms the conversion of HSQ molecules from cage-like configuration to network-like configuration post-EUV exposure.

The Si—O cage and Si—O network slopes in Figure 5 can be extrapolated to find an intersection point, which provides an estimate of the EUV sensitivity of the resist. For HSQ resist, the intersection point lies at a high dose of approximately 180 mJ/cm^2 , which means that its cages require a high EUV dose to cross-link sufficiently to produce patterns.

2.1.3. Electron-Induced Desorption from HSQ Films. Freshly deposited HSQ films of 40 nm thickness were exposed to electrons of fixed energy over the range from 2 to 70 eV. As can be seen in Figure 6, the electron exposure of the films at incident electron energies above 4 eV results in the desorption of hydrogen and silane as the predominant species, which was the same observation made when HSQ films were exposed to EUV light. The desorption rate of hydrogen and silane is monitored as a function of the electron energy (Figure 6), along with the desorption rate of CO₂ as a reference. The onset of electron-induced desorption of hydrogen and silane from the HSQ films is around 4 eV; a shoulder is observed on the onset curves at around 8 eV and a clear, fairly sharp peak with a maximum at around 11 eV. These observations are the same for hydrogen and silane desorption.

2.1.4. Quantum Chemical Calculations. To gain better insights into the underlying secondary electron-induced processes leading to the observed desorption, thermo-chemical

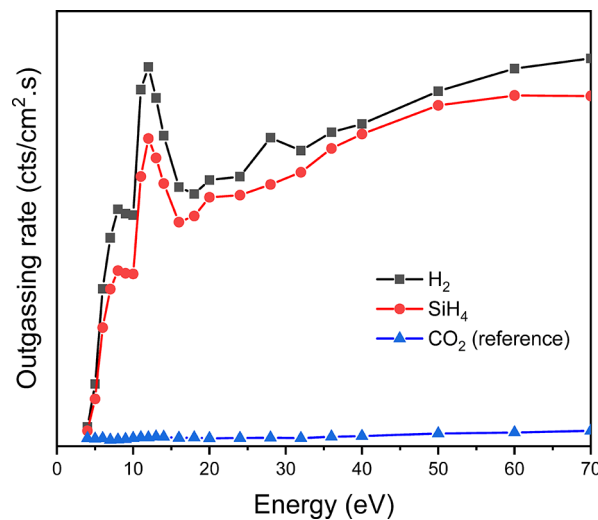
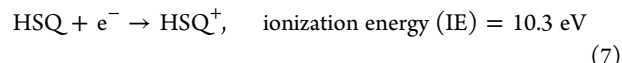
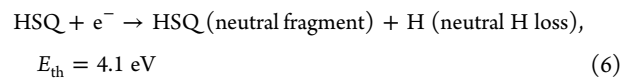
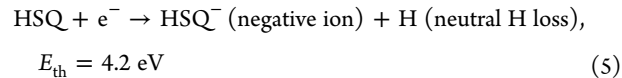


Figure 6. Electron-induced desorption rate of H₂ and SiH₄ from 40 nm-thick HSQ films.

threshold calculations were carried out for dissociative electron attachment (DEA) leading to neutral hydrogen loss (eq 5), for hydrogen loss through neutral dissociation (eq 6), and for the ionization of the isolated HSQ molecule (eq 7).



According to these calculations, the threshold for the neutral hydrogen loss through DEA is found to be at 4.2 eV. The threshold for hydrogen loss in neutral dissociation is found to be 4.1 eV, and the IE of HSQ is found to be 10.3 eV. It is thus clear that ND or DEA must be responsible for the desorption below 10 eV. Among these processes, DEA is a resonant process observed within fairly narrow energy ranges while ND is nonresonant appearing through a fairly sharp onset before leveling off at higher energies. There are no clear peaks observed in the onset region, which reflects an underlying resonant process, which in turn indicates that ND rather than DEA is responsible for the bulk of the desorption observed below about 8 eV. However, the structure at around 8 eV may be explained by additional contribution through DEA in that energy range. In general, DI sets in slightly above the ionization energy of the respective molecule, and this reaction channel might be responsible for the sharp rise in the desorption observed slightly above 10 eV (Figure 6). However, DI, like ND, is a nonresonant process and the distinct peak observed close to 11 eV cannot be explained by DI alone. A definitive explanation of this structure could not be determined, but most likely, it reflects DEA from a high lying core excited shape resonance that is stabilized through polarization interaction in the condensed media.

From the mechanistic studies, it is clear that the HSQ molecules interact strongly with the secondary electrons through multiple fragmentation pathways. However, it suffers from two major issues, (i) low EUV absorption and (ii) low

TMAH developer solubility, which severely affect its EUV printability. Therefore, HSQ cages are chemically engineered to overcome these issues.

2.2. Engineered HSQ-Based Systems. To improve the developer sensitivity of the HSQ molecule, some of the Si—H bonds in HSQ cages were replaced with Si—OH groups. This improved the solubility of HSQ cages in the TMAH developer solvent. Silanol groups also contain oxygen atoms, which have a higher EUV absorption as compared to Si and H atoms³⁶ and thus help in improving the EUV absorption of the engineered system. To further improve the EUV sensitivity of HSQ cages, it is also possible to use partially cross-linked HSQ cages as a starting material. A combination of these two methods is used to engineer a more sensitive partially cross-linked silanol-functionalized HSQ-type resist system for the EUVL process (called engineered system 1). The structure of engineered system 1 can be found in Figure S4 in the Supporting Information.

FTIR analysis of system 1 validated its improved EUV sensitivity compared to the original HSQ cages, as confirmed by the Si—O cage and Si—O network slope intersection at a dose of around 60 mJ/cm² (Figure 7).

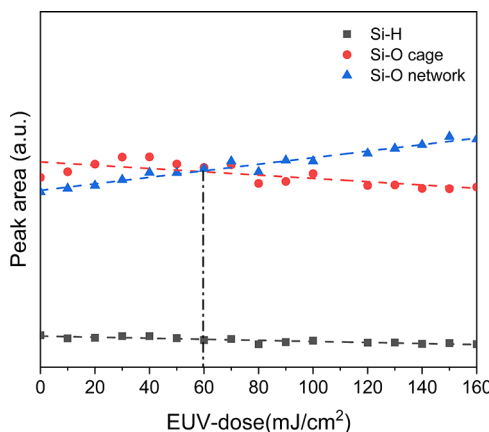


Figure 7. Si—O cage and network peak areas of engineered system 1 show a better EUV sensitivity with the intersection point at a dose of 60 mJ/cm².

Next, 16 nm dense L/S patterns were checked with the standard 2.38% v/v TMAH developer for the 20 nm-thick film of this system. However, the results were similar to the simple HSQ system, that is, the patterns were not completely resolved and the spaces were not clean (SEM image provided in Figure S5 in the Supporting Information). Therefore, a more potent 5% v/v TMAH developer was used for 100 s to resolve different L/S patterns in the Imec's ASML NXE3300B scanner. As seen from the SEM images in Figure 8, the 5% v/v TMAH developer is strong enough to resolve 16 and 20 nm dense L/S patterns with a dose of 70 mJ/cm². The 16 nm lines showed quite a lot of pinching and high line-edge roughness (LER), but 20 nm patterns were relatively smooth with an average LER value of 4.9 nm.

The next step to further improve system 1 was to make it more sensitive to the TMAH developer so that 2.38% v/v TMAH becomes efficient enough to open up dense patterns. This is because of two reasons: (i) most of the litho-tracks engineering is optimized for processing with 2.38% TMAH (as it is a common PTD in the semiconductor industry) and not

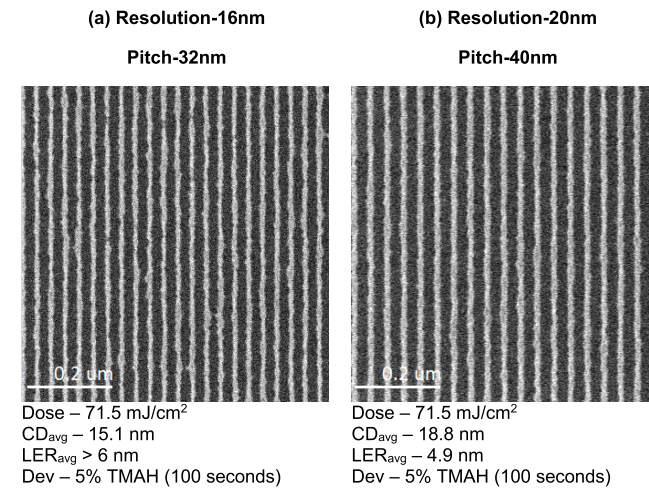


Figure 8. SEM images (at 53K magnification) of engineered system 1 at (a) 16 nm and (b) 20 nm dense L/S patterns developed with 5% v/v TMAH applied for 100 s.

with 5% v/v TMAH and (ii) 5% v/v TMAH is extremely toxic and poses a high environmental, health, and safety hazard.³⁵

Improved solubility in the TMAH developer was achieved by functionalizing the HSQ cages with carbinols (R-CH₃OH groups), which exhibit lower pKa compared to the residual silanols present in the system (engineered system 2). This increases the acidity of the cages and improves their solubility in TMAH base. EUV printability of system 2 was checked at 16 and 20 nm resolutions with the 2.38% v/v TMAH developer applied for 100 s, and the results are presented in Figure 9. From the images, it is confirmed that system 2 is now

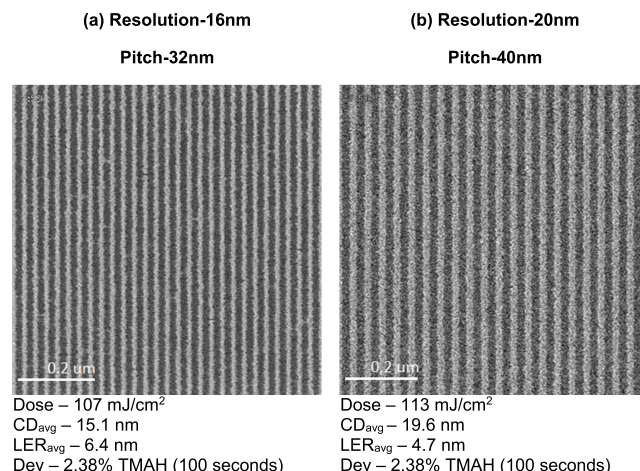


Figure 9. SEM images (at 53K magnification) of engineered system 2 at (a) 16 nm and (b) 20 nm dense line—space patterns with the 2.38% v/v TMAH developer applied for 100 s.

sensitive to 2.38% v/v TMAH to open up dense patterns. There is also a slight improvement in pattern roughness compared to system 1. However, as the acidic carbinol functional groups have vastly improved the solubility of the HSQ cages in the 2.38% TMAH developer, an EUV dose >100 mJ/cm² was now required to pattern at these high resolutions.

3. CONCLUSIONS

HSQ-based photoresist systems have already shown promising results for high-resolution patterning with electron-beam and interference lithography and therefore is an interesting material to be considered for EUV lithography. In this work, contrast curve analysis and EUV printability of simple HSQ resist are checked along with a mechanistic study to understand the ways to improve the dense (1:1) L/S patterning of the system. Contrast curve analysis of HSQ resist for the 2.38% v/v TMAH developer applied for the different time frames (30, 100, and 300 s) suggested that the image contrast is proportional to the development time. However, the EUV patterning at 16 and 22 nm dense L/S confirmed that 100 s is the optimal development time, as the longer development time (300 s) also dissolved the patterned (cross-linked) part. Upon further inspection of these patterns, it was also found that the spaces were not completely clean, which meant that 2.38% v/v TMAH was not strong enough to resolve dense patterns.

EUV-induced desorption studies of HSQ films confirmed the desorption of two major species, hydrogen and silane. Based on this, cross-linking of HSQ cages was hypothesized by two pathways through dehydrogenation and redistribution reactions. The redistribution reaction is the predominant pathway and was analyzed by FTIR spectroscopy by following Si—O (cage) and Si—O (network) peak areas. The Si—O (cage) peak area showed a linear decrease with the EUV dose, whereas the Si—O (network) peak area showed a proportional increase, confirming the conversion from closed cage-like to open network-type chemistry. Also, the intersection point at around 180 mJ/cm² for the slopes of Si—O cage and Si—O network peak areas suggested that the HSQ cages require a high EUV dose to move from cage-dominated structures to network-dominated structures.

Electron-induced desorption studies of HSQ films showed an onset of hydrogen and silane desorption at about 4 eV, a shoulder at around 8 eV, and a clear peak close to 11 eV. Quantum chemical calculations of the thresholds for individual processes showed that DI of HSQ molecules has a threshold above 10.3 eV (calculated IE of HSQ). Neutral dissociation (ND) was found to have a threshold of 4.1 eV, while the DEA reaction leading to neutral H was found to be 4.3 eV. Concerning the underlying mechanism, the current study suggested that ND through electron excitation dominates below the ionization threshold, but the structure at around 8 eV and the clear peak at around 11 eV were attributed to additional contribution through DEA. At higher energies, above the IE of HSQ, both DI and ND were likely to contribute.

To improve the litho-properties of the simple HSQ system, partially cross-linked cages were functionalized with silanol-functional groups to increase the EUV sensitivity and cage solubility in the TMAH developer solvent. This was confirmed by the intersection of the slopes of the Si—O cage and Si—O network FTIR peak areas at around 60 mJ/cm². EUV patterning of this system with 2.38% v/v TMAH was problematic as the dense features could still not be resolved. Therefore, a stronger 5% v/v TMAH developer was adopted and could resolve 16 and 20 nm dense patterns with LER values of over 6 and 4.9 nm, respectively. Further improvements in the engineered system were carried out by adding acidic carbinol functional groups that improve the TMAH solubility of the cages. As a result, the 2.38% v/v TMAH

developer could print 16 and 20 nm dense L/S patterns, with LER values of 6.4 and 4.7 nm, respectively. However, with the improvement in TMAH solubility, a high EUV dose of over 100 mJ/cm² was required to print at these resolutions. Further optimizations of the HSQ-based system would be needed to overcome the developer solubility and dose trade-off and bring it closer to high-resolution HVM by EUV lithography.

4. EXPERIMENTAL SECTION

4.1. Materials. A solution of 4% w/v HSQ resist was obtained from Dow Corning. This was diluted further in methyl isobutyl ketone solvent and spin-coated onto the silicon substrate at 2000 rpm to produce 20 and 40 nm-thick films. Engineered HSQ-type systems in which basic HSQ cages were modified to improve their EUV and TMAH developer sensitivity were obtained from the resist manufacturing company PiBond, Espoo, Finland. The detailed structures of HSQ and engineered resist systems are provided in Figures S1, S4, and S7 in the Supporting Information.

4.2. Methodology. **4.2.1. RGA/QMS Analyses of EUV- and Electron-Induced Desorption.** EUV- and electron-induced mechanisms were studied using a residual gas analyzer (RGA)/quadrupole mass spectrometer (QMS) setup installed in an Imec's outgas tool on the 40 nm-thick films.³⁷ Exposure to EUV radiation and electron beam causes chemical changes in the resist bulk and results in the desorption of certain volatile species. In the RGA, the desorbing species were ionized by electron impact and analyzed using a QMS to obtain a mass spectrum. The species were identified by comparing the spectrum with the NIST database.³⁸ The detailed setup and the description of the outgas tool can be obtained elsewhere.³²

4.2.2. Grazing Angle Attenuated Total Reflection–Fourier Transform Infrared (GATR-FTIR) Spectroscopy. Different chemical bonds absorb IR at different wavenumber and modes, which provides a fingerprint of the chemistry before and after EUV exposure. GATR-FTIR spectroscopy, which works on the principle of total internal reflectance⁴⁰ mode, was used to understand these chemical changes. Si wafer (300 mm) was spin-coated with the photoresist material, and different square regions (3 × 3 cm) were exposed with variable EUV doses. The exposed coupons were cut out and analyzed with an Imec's Nicolet 6700 FTIR spectrometer.

4.2.3. Quantum Chemical Calculations. All calculations were carried out using ORCA⁴¹ version 4.2.1. Due to the size of the system, only DFT with hybrid-GGA functional PBE0^{42,43} was used. The calculations refer to isolated molecules and fragments in the gas phase. Geometry optimization of the molecular structures (Cartesian coordinates of all optimized geometries are provided in Section S8 in the Supporting Information) and single-point energy calculations were carried out using density functional theory (DFT) at the PBE0/def2-TZVP,⁴⁴ for the ionization energy (of cations) and threshold of the ND process (neutral species), and PBE0/ma-def2-TZVP^{44,45} level of theory, including the D3(BJ) dispersion correction by Grimme et al.^{46,47} (using minimal augmented diffuse basis sets) for the threshold of the DEA process (anions). Harmonic vibrational frequencies were also calculated at this level and were used to derive zero-point vibrational energy and thermal energy corrections.

4.2.4. Contrast Curve Analysis and Patterning with the Imec's ASML NXE3300B EUV Scanner. The Imec's outgas tool^{37,39} with the EUV source was used to check the chemical contrast of the photoresist systems. The photoresist material was coated on a 200 mm Si wafer, and multiple points were exposed to a variable EUV dose in an open frame. The film thickness was checked with an ellipsometer. The development step was carried for a variable time on the exposed wafer with 2.38% v/v tetramethylammonium hydroxide (TMAH) to find the conditions that provide the best image contrast. Patterning experiments were conducted on 20 nm-thick films (spin-coated on 300 mm bare Si wafers) using the Imec's ASML NXE3300B EUV scanner to check the printability at different line-space (L/S) patterns. A Hitachi critical dimension-scanning electron microscope (CD-SEM) was used to analyze the patterns.

ASSOCIATED CONTENT

Supporting Information

The Supporting Information is available free of charge at <https://pubs.acs.org/doi/10.1021/acspm.1c00018>.

Molecular structures of HSQ and engineered systems; SEM analysis of HSQ and engineered systems; FTIR peaks for the redistribution pathway; and Cartesian coordinates of optimized geometries for quantum chemical calculations ([PDF](#))

AUTHOR INFORMATION

Corresponding Author

Ashish Rathore — Department of Chemistry, KU Leuven, 3001 Leuven, Belgium; IMEC, 3001 Leuven, Belgium;
orcid.org/0000-0003-3315-1588; Email: ashish.rathore@imec.be

Authors

Ivan Pollentier — IMEC, 3001 Leuven, Belgium
Maicol Cipriani — Science Institute and Department of Chemistry, University of Iceland, 107 Reykjavik, Iceland
Harpreet Singh — Centre for Nanoscience and Nanotechnology, Panjab University, 160014 Chandigarh, India
Danilo De Simone — IMEC, 3001 Leuven, Belgium
Oddur Ingólfsson — Science Institute and Department of Chemistry, University of Iceland, 107 Reykjavik, Iceland; orcid.org/0000-0002-7100-9438
Stefan De Gendt — Department of Chemistry, KU Leuven, 3001 Leuven, Belgium; IMEC, 3001 Leuven, Belgium

Complete contact information is available at: <https://pubs.acs.org/10.1021/acspm.1c00018>

Funding

This project has received funding from the European Union's Horizon 2020 research and innovation program under the Marie Skłodowska-Curie grant agreement no. 722149 with the acronym "ELENA", which provides the PhD grant funding for A.R.M.C. acknowledges the doctoral grant from the University of Iceland Research Fund.

Notes

The authors declare no competing financial interest.

ACKNOWLEDGMENTS

The authors would like to thank the photoresist manufacturing company, PiBond, for providing the engineered HSQ-based systems for this study. A.R. would like to thank Dr. Chidharth Krishnaraj for suggesting changes and improving the manuscript.

REFERENCES

- (1) Kozawa, T.; Tagawa, S. Radiation Chemistry in Chemically Amplified Resists. *Jpn. J. Appl. Phys.* **2010**, *49*, No. 030001.
- (2) Saeki, A.; Kozawa, T.; Ohnishi, Y.; Tagawa, S. Reactivity between Biphenyl and Precursor of Solvated Electrons in Tetrahydrofuran Measured by Picosecond Pulse Radiolysis in Near-Ultraviolet, Visible, and Infrared. *J. Phys. Chem. A* **2007**, *111*, 1229–1235.
- (3) Torok, J.; Del Re, R.; Herbol, H.; Das, S.; Bocharova, I.; Paolucci, A.; Ocola, L. E.; Ventrice, C., Jr.; Lifshin, E.; Denbeaux, G.; Brainard, R. L. Secondary Electrons in EUV Lithography. *J. Photopolym. Sci. Technol.* **2013**, *26*, 625–634.
- (4) Robinson, A. P. G.; Lawson, R. *Materials and Processes for Next Generation Lithography*; 2016; Vol. 11.
- (5) Narasimhan, A.; Grzeskowiak, S.; Ostrander, J.; Schad, J.; Rebeyev, E.; Neisser, M.; Ocola, L. E.; Denbeaux, G.; Brainard, R. L. Studying Electron-PAG Interactions Using Electron-Induced Fluorescence. In *Advances in Patterning Materials and Processes XXXIII*, SPIE. 2016, 9779, 97790F.
- (6) Narasimhan, A.; Grzeskowiak, S.; Ackerman, C.; Flynn, T.; Denbeaux, G.; Brainard, R. L. Mechanisms of EUV Exposure: Electrons and Holes. In *Extreme Ultraviolet (EUV) Lithography VIII*, SPIE. 2017, *10143*, 101430W.
- (7) Gronheid, R.; Younkin, T.; Leeson, M.; Fonseca, C.; Hooge, J. S.; Nafus, K.; Biafore, J.; Smith, M. Extreme-Ultraviolet Secondary Electron Blur at the 22-Nm Half Pitch Node. *J. Micro/Nanolithography, MEMS, MOEMS* **2011**, *10*, No. 033004.
- (8) Kozawa, T.; Shigaki, T.; Okamoto, K.; Saeki, A.; Tagawa, S.; Kai, T.; Shimokawa, T. Analysis of Acid Yield Generated in Chemically Amplified Electron Beam Resist. *J. Vac. Sci. Technol. B Microelectron. Nanom. Struct.* **2006**, *24*, 3055.
- (9) Tsubaki, H.; Tarutani, S.; Inoue, N.; Takizawa, H.; Goto, T. EUV Resist Materials Design for 15 Nm Half Pitch and Below. *J. Photopolym. Sci. Technol.* **2013**, *26*, 649–657.
- (10) Tarutani, S.; Tamaoki, H.; Tsubaki, H.; Takahashi, T.; Takizawa, H.; Takahashi, H.; Kang, S.-J. Characterizing Polymer Bound PAG Type EUV Resist. *J. Photopolym. Sci. Technol.* **2011**, *24*, 185–191.
- (11) Li, L.; Liu, X.; Pal, S.; Wang, S.; Ober, C. K.; Giannelis, E. P. Extreme Ultraviolet Resist Materials for Sub-7 nm Patterning. *Chem. Soc. Rev.* **2017**, *46*, 4855–4866.
- (12) Trikeriotis, M.; Bae, W. J.; Schwartz, E.; Krysak, M.; Lafferty, N.; Xie, P.; Smith, B.; Zimmerman, P. A.; Ober, C. K.; Giannelis, E. P. Development of an Inorganic Photoresist for DUV, EUV, and Electron Beam Imaging. In *Advances in Resist Materials and Processing Technology XXVII*, SPIE; 2010, 7639, 76390E.
- (13) Trikeriotis, M.; Krysak, M.; Chung, Y. S.; Ouyang, C.; Cardineau, B.; Brainard, R.; Ober, C. K.; Giannelis, E. P.; Cho, K. A New Inorganic EUV Resist with High-Etch Resistance. In *Extreme Ultraviolet (EUV) Lithography III*, SPIE; 2012, 8322, 83220U.
- (14) Trikeriotis, M.; Krysak, M.; Chung, Y. S.; Ouyang, C.; Cardineau, B.; Brainard, R.; Ober, C. K.; Giannelis, E. P.; Cho, K. Nanoparticle Photoresists from HfO₂ and ZrO₂ for EUV Patterning. *J. Photopolym. Sci. Technol.* **2012**, *25*, 583–586.
- (15) Ekinci, Y.; Vockenhuber, M.; Hojeij, M.; Wang, L.; Mojarrad, N. Evaluation of EUV Resist Performance with Interference Lithography towards 11 Nm Half-Pitch and Beyond. In *Extreme Ultraviolet (EUV) Lithography*, SPIE; 2013, 8679, 867910.
- (16) Toriumi, M.; Sato, Y.; Kumai, R.; Yamashita, Y.; Tsukiyama, K.; Itani, T. Characterization of "metal Resist" for EUV Lithography. In *Advances in Patterning Materials and Processes XXXIII*, SPIE; 2016, 9779, 97790G.
- (17) Castellanos Ortega, S.; Wu, L.; Baljozovic, M.; Portale, G.; Kazazis, D.; Vockenhuber, M.; Ekinci, Y.; Jung, T. Ti, Zr, and Hf-Based Molecular Hybrid Materials as EUV Photoresists. In *Extrem. Ultrav. Lithogr. IX*, SPIE; 2018, 10583, 105830A.
- (18) Cardineau, B.; Del Re, R.; Marnell, M.; Al-Mashat, H.; Vockenhuber, M.; Ekinci, Y.; Sarma, C.; Freedman, D. A.; Brainard, R. L. Photolithographic Properties of Tin-Oxo Clusters Using Extreme Ultraviolet Light (13.5 Nm). *Microelectron. Eng.* **2014**, *127*, 44–50.
- (19) Thakur, N.; Vockenhuber, M.; Ekinci, Y.; Castellanos, S. Zinc-Based Metal Oxoclusters: Towards Enhanced EUV Absorptivity. In *Extreme Ultraviolet (EUV) Lithography X*, SPIE; 2019, 10957, 109570D.
- (20) Luo, C.; Xu, C.; Lv, L.; Li, H.; Huang, X.; Liu, W. Review of Recent Advances in Inorganic Photoresists. *RSC Adv.* **2020**, *10*, 8385–8395.
- (21) Grenville, A.; Anderson, J. T.; Clark, B. L.; De Schepper, P.; Edson, J.; Greer, M.; Jiang, K.; Kocsis, M.; Meyers, S. T.; Stowers, J. K.; Telecky, A. J. Integrated Fab Process for Metal Oxide EUV

- Photoresist. In *Advances in Patterning Materials and Processes XXXII*, SPIE; 2015, 9425, 94250S.
- (22) Yang, J. K. W.; Berggren, K. K. Using High-Contrast Salty Development of Hydrogen Silsesquioxane for Sub-10-Nm Half-Pitch Lithography. *J. Vac. Sci. Technol., B: Microelectron. Nanometer Struct.-Process., Meas., Phenom.* **2007**, *25*, 2025–2029.
- (23) Lister, K. A.; Casey, B. G.; Dobson, P. S.; Thomas, S.; Macintyre, D. S.; Wilkinson, C. D. W.; Weaver, J. M. R. Pattern Transfer of a 23 Nm-Period Grating and Sub-15 Nm Dots into CVD Diamond. *Microelectron. Eng.* **2004**, *73-74*, 319–322.
- (24) Nakamatsu, K.-I.; Watanabe, K.; Tone, K.; Katase, T.; Hattori, W.; Ochiai, Y.; Matsuo, T.; Sasago, M.; Namatsu, H.; Komuro, M.; Matsui, S. Bilayer Resist Method for Room-Temperature Nanoimprint Lithography. *Jpn. J. Appl. Phys.* **2004**, *43*, 4050.
- (25) van Delft, F. C. M. J. M.; Weterings, J. P.; van Langen-Suurling, A. K.; Romijn, H. Hydrogen Silsesquioxane/Novolak Bilayer Resist for High Aspect Ratio Nanoscale Electron-Beam Lithography. *J. Vac. Sci. Technol., B: Microelectron. Nanometer Struct.-Process., Meas., Phenom.* **2000**, *18*, 3419–3423.
- (26) Fan, D.; Ekinici, Y. Photolithography Reaches 6 Nm Half-Pitch Using EUV Light. In *Extrem. Ultrav. Lithogr. VII*, SPIE; 2016, 9776, 97761V.
- (27) Desai, V.; Mellish, M.; Bennett, S.; Cady, N. C. Process Development for High Resolution Hydrogen Silsesquioxane Patterned Using a Commercial Scanner for Extreme Ultraviolet Lithography. *J. Vac. Sci. Technol., B: Microelectron. Nanometer Struct.-Process., Meas., Phenom.* **2017**, *35*, No. 021603.
- (28) Yang, C.-C.; Chen, W.-C. The Structures and Properties of Hydrogen Silsesquioxane (Hsq) Films Produced by Thermal Curing. *J. Mater. Chem.* **2002**, *12*, 1138–1141.
- (29) Olynick, D. L.; Cord, B.; Schipotin, A.; Ogletree, D. F.; Schuck, P. J. Electron-Beam Exposure Mechanisms in Hydrogen Silsesquioxane Investigated by Vibrational Spectroscopy and *in Situ* Electron-Beam-Induced Desorption. *J. Vac. Sci. Technol., B: Microelectron. Nanometer Struct.-Process., Meas., Phenom.* **2010**, *28*, 581–587.
- (30) Namatsu, H.; Takahashi, Y.; Yamazaki, K.; Yamaguchi, T.; Nagase, M.; Kurihara, K. Three-Dimensional Siloxane Resist for the Formation of Nanopatterns with Minimum Linewidth Fluctuations. *J. Vac. Sci. Technol., B: Microelectron. Nanometer Struct.-Process., Meas., Phenom.* **1998**, *16*, 69–76.
- (31) Ingólfsson, O. *Low Energy Electrons: Fundamentals and Applications*; CRC Press: Boca Raton, FL, 2019.
- (32) Junarsa, I.; Stoykovich, M. P.; Nealey, P. F.; Ma, Y.; Cerrina, F.; Solak, H. H. Hydrogen Silsesquioxane as a High Resolution Negative-Tone Resist for Extreme Ultraviolet Lithography. *J. Vac. Sci. Technol., B: Microelectron. Nanometer Struct.-Process., Meas., Phenom.* **2005**, *23*, 138–143.
- (33) Kim, J.; Chao, W.; Griedel, B.; Liang, X.; Lewis, M.; Hilken, D.; Olynick, D. Understanding the Base Development Mechanism of Hydrogen Silsesquioxane. *J. Vac. Sci. Technol., B: Microelectron. Nanometer Struct.-Process., Meas., Phenom.* **2009**, *27*, 2628–2634.
- (34) Bornhauser, P.; Calzaferri, G. Normal Coordinate Analysis of $H_8Si_8O_{12}$. *Spectrochim. Acta, Part A* **1990**, *46*, 1045–1056.
- (35) Lee, C.-H.; Wang, C.-L.; Lin, H.-F.; Chai, C.-Y.; Hong, M.-Y.; Ho, C.-K. Toxicity of Tetramethylammonium Hydroxide: Review of Two Fatal Cases of Dermal Exposure and Development of an Animal Model. *Toxicol. Ind. Health* **2011**, *27*, 497–503.
- (36) Henke, B.L.; Gullikson, E.M.; Davis, J.C. X-ray interactions: photoabsorption, scattering, transmission, and reflection $E = 50\text{--}30,000 \text{ eV}$, $Z = 1\text{--}92$. *At. Data Nucl. Data Tables* **1993**, *54* (2), 181–342.
- (37) Pollentier, I.; Vesters, Y.; Jiang, J.; Vanelderen, P.; De Simone, D. Unraveling the Role of Secondary Electrons upon Their Interaction with Photoresist during EUV Exposure. *Proc. SPIE* **2017**, *10450*, 10450H.
- (38) NIST chemistry webbook <https://webbook.nist.gov/chemistry/>.
- (39) Pollentier, I.; Aksnov, G.; Goethals, A.-M.; Gronheid, R.; Jonckheere, R.; Leeson, M. Measurement and Analysis of EUV Photoresist Related Outgassing and Contamination. *Altern. Lithogr. Technol.*, SPIE; 2009, 7271, 727146.
- (40) Fahrenfort, J. Attenuated Total Reflection: A New Principle for the Production of Useful Infra-Red Reflection Spectra of Organic Compounds. *Spectrochim. Acta* **1961**, *17*, 698–709.
- (41) Neese, F. The ORCA Program System. *WIREs Comput. Mol. Sci.* **2012**, *2*, 73–78.
- (42) Perdew, J. P.; Burke, K.; Ernzerhof, M. Generalized Gradient Approximation Made Simple. *Phys. Rev. Lett.* **1996**, *77*, 3865.
- (43) Adamo, C.; Barone, V. Toward Reliable Density Functional Methods without Adjustable Parameters: The PBE0 Model. *J. Chem. Phys.* **1999**, *110*, 6158–6170.
- (44) Weigend, F.; Ahlrichs, R. Balanced Basis Sets of Split Valence, Triple Zeta Valence and Quadruple Zeta Valence Quality for H to Rn: Design and Assessment of Accuracy. *Phys. Chem. Chem. Phys.* **2005**, *7*, 3297–3305.
- (45) Zheng, J.; Xu, X.; Truhlar, D. G. Minimally Augmented Karlsruhe Basis Sets. *Theor. Chem. Acc.* **2011**, *128*, 295–305.
- (46) Grimme, S.; Ehrlich, S.; Goerigk, L. Effect of the Damping Function in Dispersion Corrected Density Functional Theory. *J. Comput. Chem.* **2011**, *32*, 1456–1465.
- (47) Grimme, S.; Antony, J.; Ehrlich, S.; Krieg, H. A Consistent and Accurate Ab Initio Parametrization of Density Functional Dispersion Correction (DFT-D) for the 94 Elements H–Pu. *J. Chem. Phys.* **2010**, *132*, 154104.